A hydrogel-based antifouling solar evaporator for highly efficient water desalination

Journal:	*Energy & Environmental Science*
Manuscript ID	EE-COM-02-2018-000567.R1
Article Type:	Communication
Date Submitted by the Author:	17-May-2018

Complete List of Authors:	Zhou, Xingyi; The University of Texas at Austin, Materials Science and Engineering Zhao, Fei; The University of Texas at Austin, Materials Science and Engineering Guo, Youhong; The University of Texas at Austin, Materials Science and Engineering Zhang, Yi; University of Science and Technology of China, Department of Chemistry Yu, Guihua; The University of Texas at Austin, Materials Science and Engineering

Energy & Environmental Science

COMMUNICATION

A hydrogel-based antifouling solar evaporator for highly efficient water desalination

Xingyi Zhou,[a,†] Fei Zhao,[a,†] Youhong Guo,[a,†] Yi Zhang,[b] and Guihua Yu[a,*]

Received 00th January 20xx,
Accepted 00th January 20xx

DOI: 10.1039/x0xx00000x

www.rsc.org/

Solar desalination is a promising method for large-scale water purification by utilizing sustainable energy. However, current high-rate solar evaporation often relies on optical concentration due to the diffusion of natural sunlight which leads to inadequate energy supply. Here we demonstrate a hydrogel-based solar evaporator capable of generating vapor at a high rate of ~2.5 kg m^{-2} h^{-1} under one sun irradiation (1 kW m^{-2}), among the best values reported in the literature. Such highly efficient solar evaporation is achieved by a hybrid hydrogel composed of hydrophilic polymer framework (polyvinyl alcohol, PVA) and solar absorber (reduced graphene oxide, rGO), which has internal capillary channels. The PVA can greatly facilitate the water evaporation owing to reduced water evaporation enthalpy in hydrogel network. The rGO penetrating in the polymeric network enables efficient energy utilization. The capillary channels sustain an adequate water supply for continuous solar vapor generation at a high rate. Such hydrogel-based solar evaporator also exhibits the promising antifouling property, enabling long-time water desalination without recycling. The high-efficiency hydrogel-based solar vapor generators open significant opportunities to enhance solar water evaporation performance and reduce the cost of solar desalination systems.

Broader context

Billions of people around the world are suffering from lack of freshwater while seawater covers 70 % area of our planet. Developing a scalable and eco-friendly technology for seawater desalination is crucial to meet the vast and increasing demand for freshwater. The solar evaporation enabled water desalination is a promising strategy for the large-scale seawater purification by utilizing sustainable energy as the only energy source. However, currently achieving high-rate solar evaporation has to rely on concentrated solar power by costly optical accessories. Here we report a novel design of highly efficient hydrogel-based solar vapor generator with water evaporation rate of 2.5 kg m^{-2} h^{-1} under one sun (1 kW m^{-2}), achieved by the tailored water transport, effective light adsorption and energy confinement within the designed hybrid hydrogels. In addition, the antifouling functionality offered by our hydrogel-based evaporators holds the promise for practical applications.

Introduction

Freshwater scarcity is one of the most serious threats to the development of human civilization.[1, 2] Among various strategies to alleviate the issue of freshwater shortage, seawater desalination offers an adequate production of high-quality water without impairing natural freshwater ecosystems.[3] Compared with traditional seawater purification technologies, such as reverse osmosis and ion exchange, some novel distillation systems have demonstrated the promising potential of evaporation-based water purification due to high efficiency, low cost and scalability.[4] In this context, exploring sustainable solar energy to power the water evaporation becomes a rapidly growing research direction.[5] Tremendous attention has been paid to increase the efficiency of solar desalination, where the key design principles can be generally summarized as follows: (*I*) enhancing the solar absorption to harvest energy from concentrated sunlight; (*II*) confining the converted energy to the small amount of water at the evaporation surface.[6-8] For instance, various absorbers with broadband and enhanced light absorption, such as ultra-black semiconductors,[9] and

[a] *Materials Science and Engineering Program and Department of Mechanical Engineering, The University of Texas at Austin, Austin, Texas 78712, USA, E-mail: ghyu@austin.utexas.edu.*
[b] *Department of Materials Science and Engineering, University of Science and Technology of China, Hefei, Anhui 230026, China.*
† These authors contributed equally.
Electronic Supplementary Information (ESI) available. See

plasmonic nanoparticles,[10-14] have been investigated for vapor generation under concentrated solar irradiation. However, despite the high evaporation rate, large-scale application of such materials or designs is hindered by the relatively low energy efficiency and the high cost of complex optical concentrators.[11] In addition to light concentration, improving energy confinement by heat localization

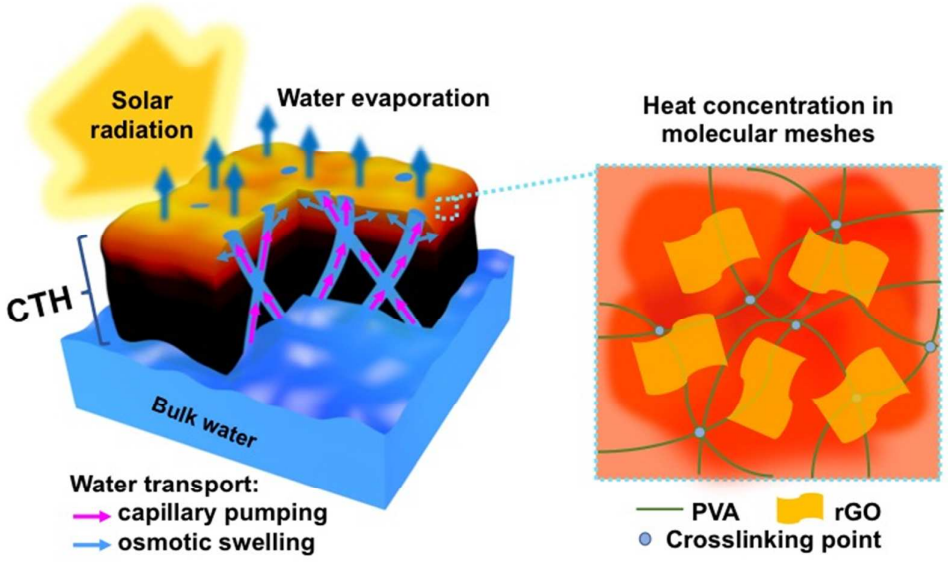

Fig. 1 Schematic illustration of solar vapor generation based on hybrid hydrogels with capillarity facilitated water transport (CTH). Upon exposure to the solar radiation, strong water evaporation (blue arrows) can be powered by solar energy. The floating CTH is capable of transporting the water from bulk water to the evaporation surface assisted with both capillary pumping (pink arrows) and osmotic swelling (light blue arrows) effects, alleviating the water loss during evaporation. rGO absorbers, interpenetrating within the polymeric network (PVA), can efficiently harvest solar energy as well as transfer and confine energy to the molecular meshes on the evaporation surface where the water evaporation is facilitated, further accelerating the water evaporation.

(converted from solar energy) has been realized with carbon-based materials,[15-18] conjugated polymers,[19] and bio-inspired nano-/micro- structures[20, 21] to achieve the solar desalination under one sun irradiation (1kW m^{-2}), opening the possibility for practical water purification under natural conditions.[22] The major challenges of these solar evaporators are (1) separating the evaporation surface from bulk water to suppress heat loss, (2) sustaining an adequate water supply from bulk water to the evaporating surface for continuous evaporation, and (3) maintaining a low water content at the evaporating surface to reduce energy consumption of water heating.[23-27]

Hydrogels, a unique class of polymer materials with 3D cross-linked polymeric networks swollen with water molecules, have been widely used in various applications because of their novel physical and chemical properties.[28, 29, 30] More importantly, it has been demonstrated that the water evaporation from hydrogels can be greatly accelerated by polymeric networks.[31, 32] Ideally, if the solar energy can be converted and confined in the molecular meshes which are located at the evaporating surface of hydrogels, the water evaporation would be greatly accelerated. However, in view of inadequate water transport in the hydrogel, the inefficient water replenishment of the evaporating molecular meshes becomes a significant challenge hindering the development of highly efficient hydrogel-based solar evaporators for practical water desalination.

Here we develop a high-efficiency solar water vapor generator based on a novel hybrid hydrogel with the enhanced water transport that is enabled by the capillary water pathways (i.e. Hydrogel with Capillarity facilitated water Transport, denoted as CTH). The CTH is constructed by penetrating reduced graphene oxide (rGO), a widely-used absorber exhibiting a broadband absorption over the full solar spectrum,[16, 26, 27] into the polymeric network of polyvinyl alcohol (PVA). As shown in Fig. 1, the strong water evaporation on the surface of CTH can be powered by solar energy. The solar heating effect is localized in a thin layer near the evaporation surface, which is insulated from bulk water, decreasing energy loss. Moreover, the water transport based on capillary pumping and osmotic swelling effects enables an adequate and uniform water supply to the evaporation surface, alleviating the water loss during evaporation. Due to the interpenetrating nature of rGO in the polymeric network of PVA, the solar energy harvested and converted by the absorber can be directly delivered to the small amount of water in molecular meshes where the water evaporation can be accelerated by the polymeric chains,[33] thus greatly facilitating the water evaporation. In addition, these molecular meshes enable the CTH to avoid the water evaporation induced crystalline fouling[34], hence achieving long-term solar desalination without the need of recycling based on the CTH. Taking advantages of the above merits, a high water evaporation rate of 2.5 kg m^{-2} h^{-1} is achieved under one sun illumination, which is the best record compared with those previously reported. Furthermore,

the potential application of such low-cost and scalable CTHs is demonstrated by a continuous solar desalination for 96h showing a very high yet stable efficiency.

Results and discussion

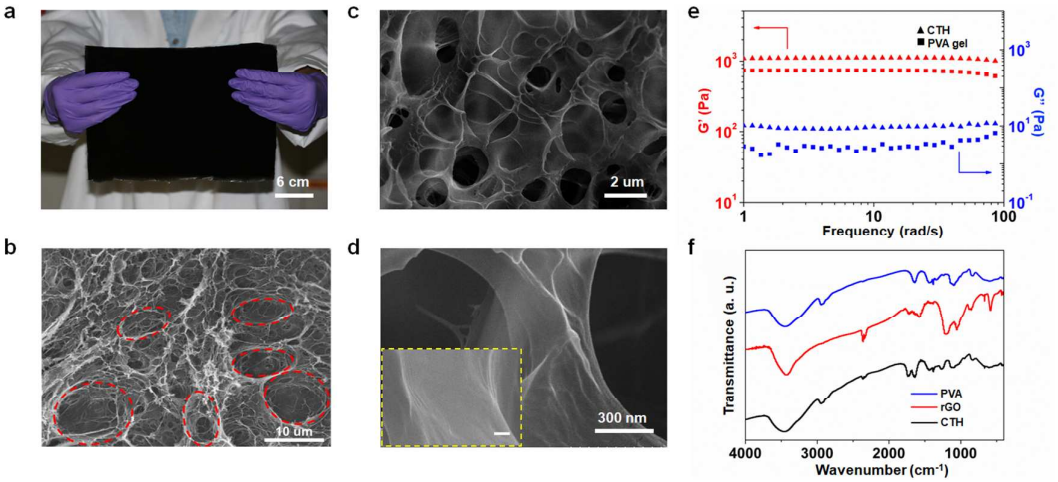

Fig. 2 Chemical and Structural Characterization of the CTH. (a) Photograph of a large piece (20 X 30 cm) of as-prepared CTH; (b-d) SEM images in different magnification showing (b) cross-section image of capillary channels from top-view (c) micron-sized pores and (d) distorted surface of the wall structure of the CTH. Inset of (d): flat surface of the wall structure in pure PVA hydrogel, scale bar is 100 nm. (e) Dynamic mechanical analysis showing storage modulus (G') and loss modulus (G") of PVA and CTH. (f) FTIR spectra of PVA, rGO and the CTH showing the chemical composition.

were investigated by the scanning electron microscopy (SEM). Fig. 2b shows the cross-section of the capillary channels inside the CTH with a diameter of about tens of microns, which is profiled by red dashes. In addition, the small pores distributing on the wall structure of capillary channels can be found with a diameter of several microns (Fig. 2c). Fig. 2d shows the roughened surface of the wall with rGO in the network of PVA, compared with the flat smooth surface of pure PVA hydrogel (Inset of Fig. 2d). Considering a swelling ratio (ca. 270 %) of the fully hydrated wall structure (Fig. S1, ESI†), the width of the capillary channels in fully hydrated CTHs is estimated to be several microns. These hierarchically interconnected capillary channels can facilitate the internal water transport of the CTH.

Owing to their viscoelasticity, the hydrogels present both energy storage and dissipation under oscillatory stress[35]. The rheology characterization, which is represented by storage modulus (G') and loss modulus (G"), can reflect the interaction among the components of the polymeric network in the CTHs. Fig. 2e shows the G' and G" values of the CTH and a pure PVA gel. The dynamic frequency sweep experiments of both gels show a wide linear viscoelastic region. The higher storage modulus compared with loss modulus confirms the cross-linked polymeric skeleton of these two gels. The G' and G" values of the CTH are higher than those of the pure PVA hydrogel, indicating extra physical cross-linking points[36] relative to PVA hydrogel due to the interaction between rGO and PVA chains. These results demonstrate that the rGOs are penetrated in the polymeric network of PVA hydrogels. Such structure is significant for efficient energy utilization (*vide infra*).

In order to analyze the chemical composition of the CTH, the Fourier-Transform infrared (FTIR) spectra of PVA, rGO, and the CTH were shown in Fig. 2f. The spectrum of PVA (blue curve) shows the absorption signal at 1110 cm^{-1}, which can be attributed to the C-O stretching and is a characteristic peak of PVA.[37] In the spectrum of rGO (red curve), the peak located at 1674 cm^{-1} corresponds to the C=C stretching in the aromatic rings.[36] All the characteristic peaks of PVA and rGO can be found in the spectrum of the CTH (black curve), confirming the presence of rGO in the PVA polymeric network. And the results of thermogravimetric analysis (TGA) as shown in Fig. S2 (ESI†), are also in agreement with the above data.

To systematically assess the influence of rGO additive on the water content and transport in CTHs, the CTHs constructed by PVA and rGOs with different carbon/oxygen ratio (i.e. C/O ratio, corresponding to different hydrophilicity, see Fig. S3, ESI†) were investigated. The CTHs are denoted as CTH1, CTH2, CTH3 and CTH4 according to the rGO with C/O ratio of 132.3, 19.6, 12.7 and 4.9, respectively. The water content (Q) is represented by

$$Q = W / W_d \quad (1)$$

where W and W_d are the weights of the water in the swollen sample and the corresponding dried aerogel sample, respectively. The swelling capacity of the CTH can be evaluated by the saturated water content (Q_s). As shown in Fig. 3a, the Q_s values from CTH1 to CTH4 are 1.95, 2.36, 2.67 and 2.86 g per gram of the corresponding xerogel (i.e. g g^{-1}), respectively, indicating that the Q_s of the CTHs can be tuned by the oxygen-containing level of rGO additives. In addition, the water transport in CTHs is evaluated by the dynamic analysis of their swelling process. Given that the CTHs are nearly completely hydrated during solar vapor generation, the swollen time from the half-saturated state (i.e. 0.5 Q_s) to the saturated state (i.e. Q_s) can reveal the water transport in the CTHs (Fig. 3b). As shown in Fig. S4 (ESI†), all the Q values of CTH1 to CTH4 present

linear dependence over time during the swelling. The water transport rate (V) can be calculated by

$$V = 0.5\ Q_s / t \quad (2)$$

where t is the half-swollen time (blue points in Fig. 3b). Upon one gram of xerogel, the CTH1, CTH2, CTH3 and CTH4 show the V of 0.008, 0.014, 0.018 and 0.029 g min^{-1}, indicating the tunable water transport property of CTHs (also see Fig. S5, ESI†). Note that the water residual in capillary channels was pre-removed by the absorbent paper in all the measurements mentioned above.

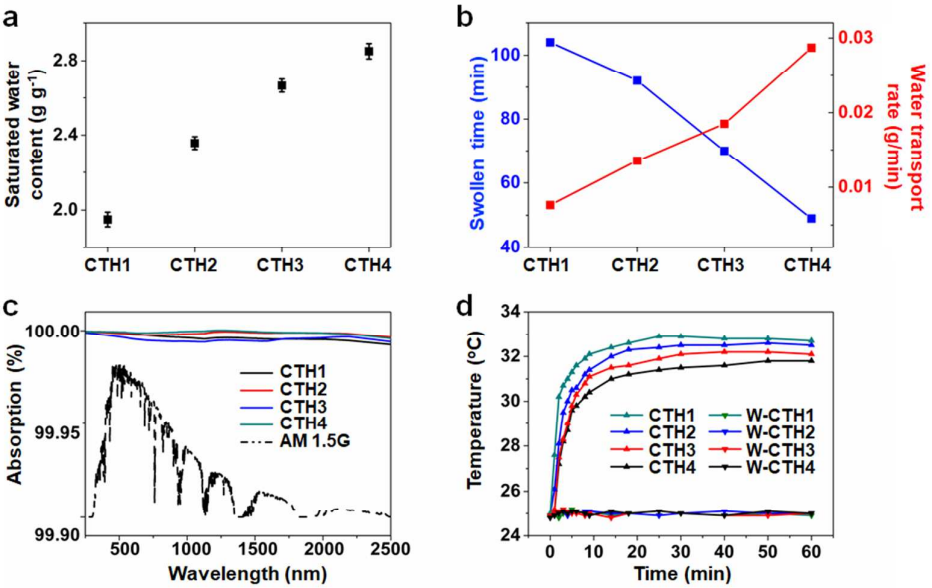

Fig. 3. Tunable water transport, solar absorption and solar thermal conversion of the CTHs. (a) The saturated water content in CTHs per gram of corresponding xerogel (i.e. g g^{-1}). The CTH1 to CTH4 represent gels containing rGO with the C/O ratio of 132.3, 19.6, 12.7 and 4.9, respectively. (b) The swollen behavior of CTHs from half-saturated to saturated state and calculated water transport rate indicate the tunable water transport in CTHs. (c) UV-vis-NIR spectra of CTH sheets with a thickness of ca. 1 mm. The normalized spectral solar irradiance density of air mass 1.5 global (AM 1.5 G) solar spectrum is shown by the black dashed line. (d) The temperature of evaporation surface in CTHs and bulk water under one sun irradiation over time. W-CTH1,2,3 and 4 represent the temperature of bulk water underneath CTH 1,2,3 and 4, respectively.

To investigate the solar absorption ability, UV-vis-NIR spectrophotometer was used to measure the light absorption of CTHs. As shown in Fig. 3c, the CTHs present excellent full solar spectrum light absorption with a negligible optical loss. In addition, the CTHs showed low reflectance in the wavelength range from 250 to 2500 nm (Fig. S6a, ESI†). These results indicate that the light absorption of the CTHs does not depend on the Q and V values, ensuring stable solar energy harvesting for vapor generation. In order to quantitatively analyse the light absorption, the transmittance of CTHs with different thicknesses were carefully measured by the UV-vis-NIR spectrophotometer. A CTH sheet with a thickness of ca. 400 μm provides average transparency of ca. 2% (Fig. S6b, ESI†), indicating efficient solar energy harvesting of CTH. To investigate the photothermal behaviour of the CTH under one sun, the temperature variations of CTH surface and bulk water were carefully traced (Fig. 3d). The free-floating CTHs show a rapid surficial temperature increase within 5 min, while the temperature of bulk water remains nearly constant. The CTHs 1-4 present similar equilibrate temperature of ca. 32 °C, while the temperature of the bulk water is found to be maintained ~ 25°C in 1 h, evidencing the effective energy confinement in the CTHs.

To measure the efficiency of solar vapor generation, the CTHs free-floating on the bulk water were exposed to solar radiation (1 kW m^{-2}) for a typical vapor generation test (Fig. 1). As the water continuously escaped from the surface of the CTH to the air under constant solar illumination, the overall mass change with and without the CTHs was recorded once the temperature reached steady state (pre-heating for ca. 30 min), representing the amount of evaporated water. The vapor generation rate based on the CTHs is much faster than that of pure water under one sun radiation. In addition, based on optimized PVA/water (Fig. S7 and S8, ESI†) and rGO/PVA (Fig. S9 and S10, ESI†) ratio, the CTH3 presents the highest water evaporation rate of ~2.5 kg m^{-2} h^{-1} (Fig. S11, ESI†), among all CTH 1-4 samples (Fig. 4a and Fig. S12, ES†). Compared with CTH3, CTH1 and CTH2 samples showed inefficient water transport which seriously limits the evaporation rate. Despite the fast water transport in CTH4, the excessive water content would reduce the energy utilization efficiency as more energy will be used to heat the water.[22] Note that all the experimental data of solar vapor generation were calibrated with dark evaporation data (see Experimental Section for details). The corresponding energy efficiency (η) is calculated by the following formula[22]

$$\eta = \dot{m} h_V / C_{opt} P_0 \quad (3)$$

in which $\dot{m}$ is the mass flux, h_V is the vaporization enthalpy of the water in CTHs, P_0 is the solar irradiation power of one sun (1 kW m^{-2}), and C_{opt} refers to the optical concentration on the absorber surface. It should be noted that the vaporization enthalpy of water can be reduced by the polymeric network of hydrogels.[31] The

vaporization enthalpy used here is smaller than the classic latent enthalpy of water (Fig. S13 and S14, ESI†). The CTH3 realized a high energy efficiency of up to ~95% under one sun (Fig. S15, ESI†). Since the water evaporating rate upon one sun directly reflects the promise of solar vapour generation under ambient conditions and natural sunlight, the high rate achieved by CTH3 (red sphere in Fig. 4b)[13, 16-18, 20-22, 26, 27] indicates a potential application of CTHs in practical solar vapor generation.

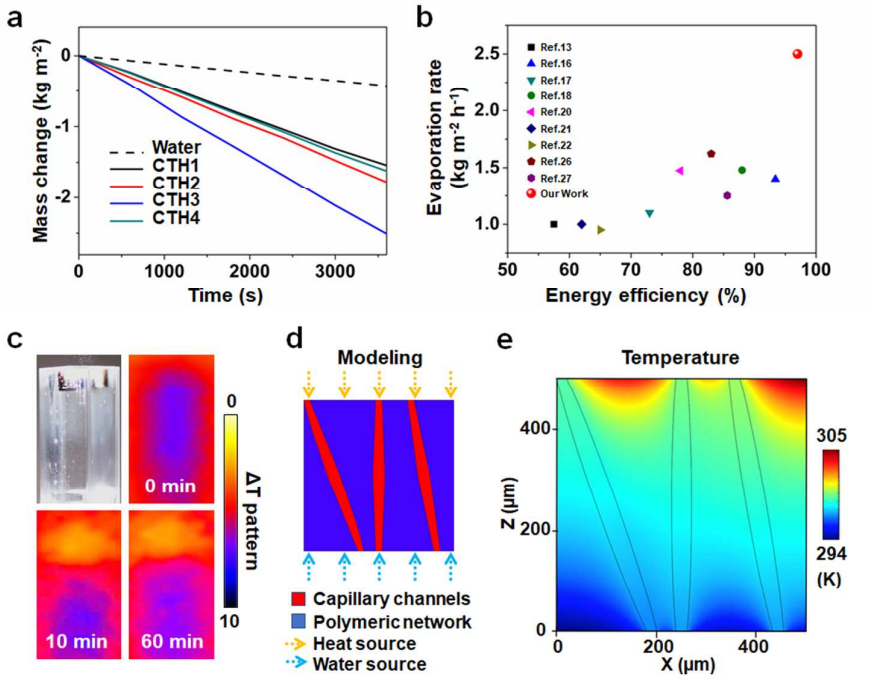

Fig. 4 Solar vapor generation of the CTH under one sun. (a) The mass loss of water for different CTH samples under one sun (1 kW m^{-2}) in comparison of pure water as the control test. (b) One-sun vapor generation performance of CTH3 compared with recent literature reports. (c) The setup for solar vapor generation test based on the CTH and corresponding infrared images showing the temperature distribution with irradiation time of 0 min, 10 min, and 60 min. (d-e) Modelling and theoretical simulation of temperature distribution near the evaporation surface of CTH, where the red olivary areas and blue background represent the capillary channels and polymeric network, respectively. The preloaded heat and water source are depicted by yellow and blue dashed arrows, respectively.

To investigate the energy utilization of CTH, infrared imaging was employed to monitor the temperature rise in the solar evaporation system (based on CTH3) under one sun radiation (Fig. 4c). The comparison of the photograph and infrared images of the solar evaporation system with exposure time of 0 min, 10 min and 60 min clearly show that the CTH is heated to ~32 °C and the temperature of bulk water is barely changed, indicating that the converted energy is confined in the CTH, rather than diffused to the bulk water. To further clarify the energy confinement near the evaporation surface, COMSOL Multiphysics was used to simulate the CTH undergoing solar radiation. Fig. 4d shows the structural modeling in which the capillary channels and polymeric network were simulated by long olivary area (red, with width of 10 μm) and quadrate background (blue) in a 2D mapping, respectively. The yellow and blue dashed arrows represent heat and water resources, respectively. A basic heat-transfer model was employed to describe temperature distribution in the CTH3 (see Supplementary Methods in ESI† for details).[11] The heat and water input were preloaded at the surface (Z = 500) and the bottom (Z = 0), respectively. After the temperature distribution reaches the steady state, the simulation results predict that the maximum temperature in the CTH can be 305 K (~32 °C) at the surface of polymeric network (Fig. 4e). This result is close to our experimental results, confirming the effective heat confinement based on the CTHs. Additionally, the biphasic mixture model was used to simulate the water transport in the CTHs to further confirm the adequate water supply (see Supplementary Methods in ESI† for details).[38] The 2D mapping of water velocity distribution depicts fast water transport through the internal gaps to recover surficial water loss (Fig. S16, ESI†).

To demonstrate the potential application, the CTH is used as the evaporator in a solar desalination system (Fig. 5a). The floating CTH harvests solar energy to vaporize the water (blue arrow). The vapor is collected as purified water through condensation, achieving the water desalination. Moreover, an equilibrium is established when the water transport induced salt ion absorption (violet arrow) and diffusion enabled salt ion discharge (yellow arrow) are balanced. To evaluate the effect of solar desalination based on CTH3, a real seawater sample (from the Gulf of Mexico) was used for desalination test, and the quality of collected purified water was measured by the inductively coupled plasma

spectroscopy (ICP). It is found that the concentration of all the four primary ions (Na^+, Mg^{2+}, K^+ and Ca^{2+}) were significantly reduced by orders (Fig. 5b) after solar desalination. In addition, three artificial seawater samples with representative salinities of the Baltic sea (0.8 wt%), world ocean (3.5 wt%) and the Dead Sea (10 wt%) were also used to evaluate the solar desalination, where the salinity of corresponding purified water decreased about four orders of magnitude (Fig. S17, ESI†). These results indicate effective solar desalination based on CTH3.

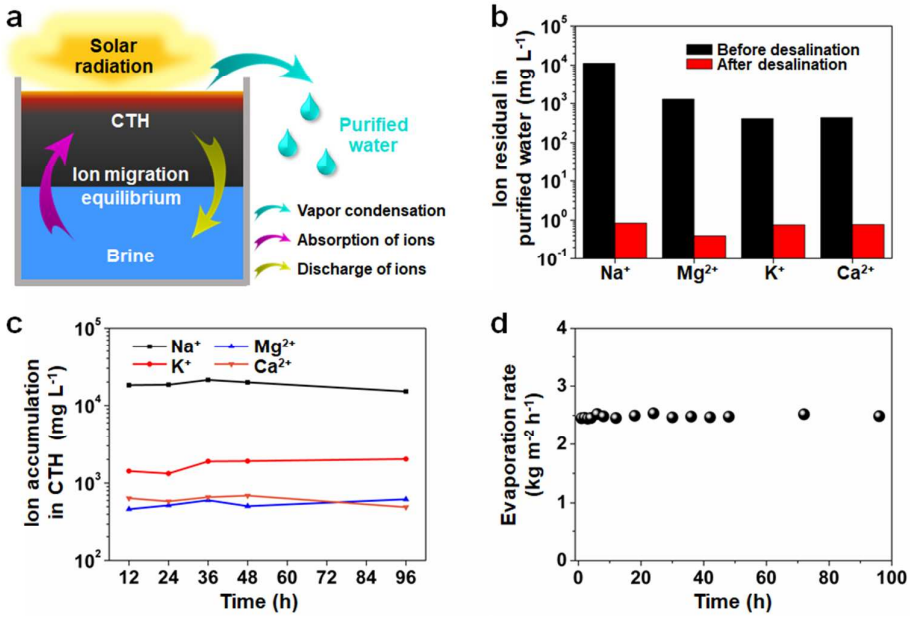

Fig. 5 CTH-based solar desalination under one sun. (a) Schematic illustration of solar desalination based on the CTH. The floating CTH harvests solar energy to vaporize the water for purification (blue arrow). An equilibrium is established when the water transport induced salt ion absorption (violet arrow) and diffusion enabled salt ion discharge (yellow arrow) are balanced. (b) Measured concentrations of four primary ions in an actual seawater sample before and after desalination. (c) Measured concentrations of four primary ions accumulated in CTHs over time, evidencing a relatively low equilibrate ion concentration in used CTH, which was not high enough to trigger the crystallization. (d) The duration test of the CTH based on a continuous solar desalination for 96 h under one sun.

The lifetime of solar evaporators, which is defined by the reusability, durability and recyclability, is another important aspect of solar desalination. As shown in Fig. 5c, the concentration of salt residual in the CTHs, is almost constant during a continuous solar desalination for 96h, suggesting the restricted ion accumulation, and hence indicating the crystalline antifouling functionality (see Fig. S18, ESI†). Furthermore, the CTH presented a stable evaporation rate under continuous one sun irradiation over 96 h (Fig. 5d) and the CTH retain its evaporation rate and antifouling property even the salinity of seawater is 20% (see Fig. S19 and S20, ESI†), showing the excellent durability toward solar irradiation and reactive salty ions. Given all above measurements, the CTH exhibited a promising solar desalination performance for long-term operation in practical environment.

Conclusions

In conclusion, highly efficient solar vapor generation has been achieved by our designed hybrid hydrogels with capillarity facilitated water transport (CTH), which offer synergistic features of tailored water transport, effective energy confinement and reduced water vaporization enthalpy. The water distribution can be regulated by the polymeric network and its interaction with rGO additives to balance the water transport and solar evaporation, hence improving the efficiency of energy utilization. More importantly, the CTH embodies a new possibility to develop high-rate solar evaporators under weak sunlight by confining the heat to the molecular meshes, and hence reducing the energy loss. Furthermore, the polymeric network can reduce the energy demand of water vaporization to facilitate the vapor generation. Such a novel design enables a solar vapor generation rate of ~ 2.5 kg m^{-2} h^{-1} with the energy efficiency of ~ 95 % under one sun irradiation. In addition, the antifouling functionality, low cost and scalability further promise the significant potential of CTHs in practical environment. Apart from the demonstrated solar water purification, the newly-developed hydrogel-based solar harvester can be used for other applications, such as environmental cooling, water/moisture management, and pollution abatement. Therefore, this work holds the promise of significantly expanding the application domain and reducing the cost of solar powered water managing systems.

Experimental Section

Materials

Chemicals including PVA with average molecular weight of 15 000, hydrochloric acid (37%), graphite powder, graphite flakes (325 mesh), potassium permanganate, sulfuric acid (98%), sodium nitrate, hydrazine monohydrate, glutaraldehyde were purchased from Sigma-Aldrich.

Fabrication of the CTH

In a typical synthesis, PVA (1 g), glutaraldehyde (125 µL, 50%wt in DI water) and DI water (10 mL) were mixed together by sonication (Solution A). Then graphene oxide (100 µL, 3% wt) and HCl (50 µL, 1.2 M) solutions were added to 1 mL of solution A, the gelation was carried out for 2 h. The obtained gel was immersed into DI water overnight to obtain pure hybrid hydrogel. The purified gel was frozen by liquid nitrogen and then thawed in DI water at a temperature of 30 °C. The freezing-thawing process was repeated 10 times. After freeze-drying, the sample was swollen with water and reduced by hydrazine with a temperature of 80 °C overnight. Finally, the CTH was washed with DI water three times to remove extra hydrazine.

Characterization

The morphology and microstructure of samples were observed by Scanning Electron Microscopy (Hitachi, S5500) operating at 5 kV. Before observation, the CTHs were freeze-dried for 24 h. The FTIR spectra of CTHs were recorded by the FTIR Spectrometer (Thermo Mattson, Infinity Gold FTIR) equipped with a liquid nitrogen cooled narrow band mercury cadmium telluride (MCT) detector, using an attenuated total reflection cell equipped with a Ge crystal. To understand the mechanical properties of the CTH, rheological experiments were performed by a rheometer (AR 2000EX, TA instrument) using parallel plate on a peltier plate in a frequency sweep mode. Absorption spectra, transparency and reflectance were recorded using a UV-VIS-NIR spectrometer (Cary 5000) with an integrating sphere unit and automation of reflectance measurement unit. The measurements were corrected by baseline/blank correction with dark correction. Note that we used hydrogel for all the relevant tests and characterization except SEM, FT-IR and TGA. The concentration of ions were tracked by inductively coupled plasma mass spectrometry (ICP-MS, Agilent 7500ce) with dilutions in 2% HNO_3 to make the loaded ion concentration lower than 10 ppm.

Solar vapor generation measurement

The water evaporation experiments were conducted in the lab with temperature of ca 25 °C and humidity of ca 45 % using a solar simulator (AbetTech, M-LS Rev B) outputting simulated solar flux at 1 kW/m^2 (1 sun). The solar flux was measured by a thermopile (Newport, 818SL) connected to a power meter (Newport, 1916-R). Because the solar flux varies across the beam spot, and the thermopile detector is about 1 cm^2 in size, the CTH was cut into small pieces with surface area of 1 cm^2 to have an accurate power input. A CTH chip with thickness of ca. 0.5 cm was floated on pure water (or brine for desalination tests) in a glass cuvette that was set to the beam spot with solar flux of 1 sun. The mass of the water loss is measured by a lab balance with 0.1 µg resolution and calibrated to weights heavier than the total weight of the setup. The dark condition-evaporation rate was subtracted from the solar-illuminated evaporation rate. All evaporation rates were measured after a stabilization under 1 sun for 30 minutes.

Conflicts of interest

There are no conflicts to declare.

Acknowledgements

The authors acknowledge the financial support from Sloan Research Fellowship, Camille-Dreyfus Teacher-Scholar Award, and National Science Foundation award (NSF-CMMI-1537894).

Notes and references

1 R. F. Service, *Science*, 2006, **313**, 1088.
2 M. Elimelech and W. A. Phillip, *Science*, 2011, **333**, 712.
3 M. A. Shannon, P. W. Bohn, M. Elimelech, J. G. Georgiadis, B. J. Mariñas and A. M. Mayes, *Nature*, 2008, **452**, 301.
4 N. S. Lewis, *Science*, 2007, **315**, 798.
5 N. S. Lewis, *Science*, 2016, **351**, 1920.
6 H. M. Qiblawey and F. Banat, *Desalination*, 2008, **220**, 633.
7 G. P. Narayan, M. H. Sharqawy, E. K. Summers, J. H. Lienhard, S. M. Zubair and M. Antar, *Renew. Sust. Energ. Rev.*, 2010, **14**, 1187.
8 C. Li, Y. Goswami and E. Stefanakos, *Renew. Sust. Energ. Rev.*, 2013, **19**, 136.
9 J. Wang, Y. Li, L. Deng, N. Wei, Y. Weng, S. Dong, D. Qi, J. Qiu, X. Chen and T. Wu, *Adv. Mater.*, 2017, **29**, 1603730.
10 O. Neumann, C. Feronti, A. D. Neumann, A. Dong, K. Schell, B. Lu, E. Kim, M. Quinn, S. Thompson and N. Grady, *Proc. Natl. Acad. Sci. U. S. A.*, 2013, **110**, 11677.
11 Y. Liu, S. Yu, R. Feng, A. Bernard, Y. Liu, Y. Zhang, H. Duan, W. Shang, P. Tao, C. Song and T. Deng, *Adv. Mater.*, 2015, **27**, 2768.
12 K. Bae, G. Kang, S. K. Cho, W. Park, K. Kim and W. J. Padilla, *Nat. Commun.*, 2015, **6**, 10103.
13 L. Zhou, Y. Tan, J. Wang, W. Xu, Y. Yuan, W. Cai, S. Zhu and J. Zhu, *Nat. Photonics*, 2016, **10**, 393.
14 C. Liu, J. Huang, C. E. Hsiung, Y. Tian, J. Wang, Y. Han and A. Fratalocchi, *Adv. Sustainable Syst.*, 2017, **1**, 1600013.
15 P. Zhang, Q. Liao, T. Zhang, H. Cheng, Y. Huang, C. Yang, C. Li, L. Jiang and L. Qu, *Nano Energy*, 2018, **46**, 415.
16 H. Ren, M. Tang, B. Guan, K. Wang, J. Yang, F. Wang, M. Wang, J. Shan, Z. Chen, D. Wei, H. Peng and Z. Liu. *Adv. Mater.*, 2017, **29,** 1702590.
17 P. Yang, K. Liu, Q. Chen, J. Li, J. Duan, G. Xue, Z. Xu, W. Xie and J. Zhou, *Energ. Environ. Sci.*, 2017, **10**, 1923.

18 Z. Liu, H. Song, D. Ji, C. Li, A. Cheney, Y. Liu, N. Zhang, X. Zeng, B. Chen, J. Gao, Y. Li, X. Liu, D. Aga, S. Jiang, A. Yu and Q. Gan, *Global Challenges*, 2017, **1**, 1600003.
19 L. Zhang, B. Tang, J. Wu, R. Li and P. Wang, *Adv. Mater.*, 2015, **27**, 4889.
20 N. Xu, X. Hu, W. Xu, X. Li, L. Zhou, S. Zhu and J. Zhu, *Adv. Mater.*, 2017, **29**, 1606762.
21 C. Chen, Y. Li, J. Song, Z. Yang, Y. Kuang, E. Hitz, C. Jia, A. Gong, F. Jiang, J. Zhu, B. Yang, J. Xie and L. Hu, *Adv. Mater.*, 2017, **29**, 1701756.
22 H. Ghasemi, G. Ni, A. M. Marconnet, J. Loomis, S. Yerci, N. Miljkovic and G. Chen, *Nat. Commun.*, 2014, **5**, 5449.
23 Y. Ito, Y. Tanabe, J. Han, T. Fujita, K. Tanigaki and M. Chen, *Adv. Mater.*, 2015, **27**, 4302.
24 G. Ni, G. Li, S. V. Boriskina, H. Li, W. Yang, T. Zhang and G. Chen, *Nat. Energy*, 2016, **1**, 16126.
25 P. Zhang, J. Li, L. Lv, Y. Zhao and L. Qu. *ACS Nano*, 2017, **11**, 5087.
26 X. Hu, W. Xu, L. Zhou, Y. Tan, Y. Wang, S. Zhu and J. Zhu, *Adv. Mater.*, 2017, **29**, 1604031.
27 Y. Li, T. Gao, Z. Yang, C. Chen, W. Luo, J. Song, E. Hitz, C. Jia, Y. Zhou, B. Liu, B. Yang and L. Hu, *Adv. Mater.*, 2017, **29**, 1700981.
28 Y. Zhao, B. Liu, L. Pan and G. Yu, *Energy Environ. Sci.*, 2013, **6**, 2856.
29 F. Zhao, Y. Shi, L. Pan and G. Yu, *Acc. Chem. Res.*, 2017, **50**, 1734.
30 Y. Shi, J. Zhang, L. Pan, Y. Shi and G. Yu, *Nano Today*, 2016, **11**, 738.
31 K. Kudo, J. Ishida, G. Syuu, Y. Sekine and T. Ikeda-Fukazawa, *J. Chem. Phys.*, 2014, **140**, 044909.
32 B. Potkonjak, J. Jovanović, B. Stanković, S. Ostojić and B. Adnadjević, *Chem. Eng. Res. Des.*, 2015, **100**, 323.
33 C. Ma, Y. Shi, D. A. Pena, L. Peng and G. Yu, *Angew. Chem., Int. Ed.*, 2015, **127**, 7484.
34 T. Geddert, W. Augustin and S. Scholl, *Heat Transfer Eng.*, 2011, **32**, 300.
35 L. Jin and R. Bai, *Langmuir*, 2002, **18**, 9765.
36 Y. Shi, D. Xiong, J. Li and N. Wang, *J. Phys. Chem. C*, 2016, **120**, 19442.
37 P. Chakraborty, P. Bairi, B. Roy and A. K. Nandi, *ACS Appl. Mater. Interfaces*, 2014, **6**, 3615.
38 E. Birgersson, H. Li and S. Wu, *J. Mech. Phys. Solids*, 2008, **56**, 444.

Energy & Environmental Science

COMMUNICATION

Graphical Abstract

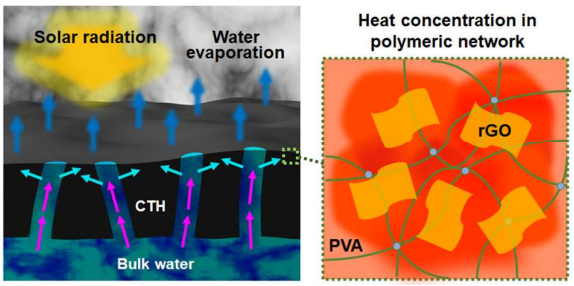

Efficient solar water evaporation was achieved by antifouling hybrid hydrogels with capillarity facilitated water transport and heat concentration in polymeric network.